ChemPubSoc Europe

DOI: 10.1002/cmdc.201700629

CHEMMEDCHEM Full Papers

Discovery and Mechanistic Elucidation of a Class of Protein Disulfide Isomerase Inhibitors for the Treatment of Glioblastoma

Anahita Kyani[+],[a] Shuzo Tamura[+],[a] Suhui Yang[+],[a] Andrea Shergalis[+],[a] Soma Samanta,[a] Yuting Kuang,[a] Mats Ljungman,[b] and Nouri Neamati*[a]

Protein disulfide isomerase (PDI) is overexpressed in glioblastoma, the most aggressive form of brain cancer, and folds nascent proteins responsible for the progression and spread of the disease. Herein we describe a novel nanomolar PDI inhibitor, pyrimidotriazinedione **35G8**, that is toxic in a panel of human glioblastoma cell lines. We performed a medium-throughput 20 000-compound screen of a diverse subset of 1 000 000 compounds to identify cytotoxic small molecules. Cytotoxic compounds were screened for PDI inhibition, and, from the screen, **35G8** emerged as the most cytotoxic inhibitor of PDI. Bromouridine labeling and sequencing (Bru-seq) of nascent RNA revealed that **35G8** induces nuclear factor-like 2 (Nrf2) antioxidant response, endoplasmic reticulum (ER) stress response, and autophagy. Specifically, **35G8** upregulated heme oxygenase 1 and solute carrier family 7 member 11 (SLC7A11) transcription and protein expression and repressed PDI target genes such as thioredoxin-interacting protein 1 (TXNIP) and early growth response 1 (EGR1). Interestingly, **35G8**-induced cell death did not proceed via apoptosis or necrosis, but by a mixture of autophagy and ferroptosis. Cumulatively, our data demonstrate a mechanism for a novel PDI inhibitor as a chemical probe to validate PDI as a target for brain cancer.

Introduction

Glioblastoma is the most common type of malignant central nervous system (CNS) tumor. Prevalence increases with age, with peak incidence in individuals aged 60–79 years.[1] Despite the treatment options available—surgical resection followed by chemoradiotherapy and adjuvant chemotherapy (temozolomide)—the five-year survival rate of patients diagnosed with glioblastoma is only 5.0%.[1,2] Current treatments are marginally effective and the number of cases is expected to grow with the aging population, emphasizing the urgent need for the development of novel and effective therapies for glioblastoma. Disease recurrence and drug resistance remain the major challenges for a successful cure.

Protein disulfide isomerase (PDI; EC 5.3.4.1) is a 57-kDa endoplasmic reticulum (ER) oxidoreductase of the thioredoxin superfamily that assists protein folding in the ER by catalyzing disulfide rearrangements (isomerase activity), disulfide formation (oxidase activity), and disulfide reduction (reductase activity).[3,4] PDI is overexpressed in several cancers but most significantly in glioblastoma.[3] Previously, we demonstrated that PDI knockdown by siRNA leads to substantial cytotoxicity in ovarian cancer cells.[5] PDI inhibitors and modulators are being developed to combat cancer and neurological diseases (for a comprehensive review of PDI inhibitors, see references [3] and [4a]). The PDI inhibitor, bacitracin, inhibits migration and invasion of glioblastoma cells[6] and enhances apoptosis caused by ER stress-inducing agents in melanoma cells.[7] Another class of compounds, T8, are weak inhibitors of PDI and at moderately high concentrations, sensitize several cancer cell lines to etoposide treatment.[8] Recently, a reversible, selective, nontoxic PDI inhibitor, ML359, was developed as a probe to study thrombosis-related diseases.[9] Modulators of PDI have also been shown to be neuroprotective. A reversible PDI modulator, LOC14 (EC_{50} = 500 nM), has neuroprotective effects in cellular and rat models of Huntington's disease.[10] Furthermore, PDI inhibitor CCF642 was demonstrated to be effective in a mouse xenograft model of multiple myeloma.[11] Mounting evidence highlights PDI as an important target against several diseases including cancer, emphasizing the need for potent, clinically relevant PDI inhibitors for cancer treatment.

Herein, we report on the development of **35G8** as a novel and potent PDI inhibitor that demonstrates activity in brain cancer cells and has drug-like properties. The activity of **35G8** in a diverse set of robust assays confirmed that the initial observation of activity was not a consequence of its redox cycling status. Results from nascent RNA Bru-seq[12] analysis showed that the transcription of 498 genes increased and 238 genes decreased at least 2-fold following a 4-hour incubation with **35G8** in U87MG glioblastoma cells. Gene set enrichment analy-

[a] *Dr. A. Kyani,[+] Dr. S. Tamura,[+] Dr. S. Yang,[+] A. Shergalis,[+] Dr. S. Samanta, Dr. Y. Kuang, Dr. N. Neamati*
Department of Medicinal Chemistry, College of Pharmacy, University of Michigan, North Campus Research Complex, 1600 Huron Parkway, Ann Arbor, MI 48109 (USA)
E-mail: neamati@umich.edu

[b] *Prof. M. Ljungman*
Departments of Radiation Oncology and Environmental Health Sciences, University of Michigan, North Campus Research Complex, 1600 Huron Parkway, Ann Arbor, MI 48109 (USA)

[+] *These authors contributed equally to this work.*

Supporting information for this article can be found under: https://doi.org/10.1002/cmdc.201700629.

sis demonstrated the upregulated genes to be involved in the Nrf2 antioxidant response and the unfolded protein response (UPR). Genes with decreased transcription involved histone and DNA repair pathways. In addition, **35G8** upregulates two key genes, SLC7A11 and HMOX1, and may kill cells through an iron-dependent form of cell death independent of apoptosis and necrosis, called ferroptosis.[13] The alterations in the transcriptional landscape induced by **35G8** provide a more comprehensive understanding of the mechanisms of PDI inhibition in brain cancer therapy.

Results and Discussion

35G8 is a nanomolar inhibitor of PDI

To identify cytotoxic small molecules, we screened a highly diverse library of 20000 compounds, representing over one million compounds, in the colon cancer cell line HCT116 (Figure 1). From the initial screen, we identified 443 cytotoxic compounds with IC_{50} values under 10 μM. These 443 compounds were tested for PDI inhibition in an insulin turbidity assay.[14] Eight compounds demonstrated potent inhibition ($IC_{50} < 1.0$ μM), and after confirming the activity with re-purchased compound stocks and verifying a dose-dependent response, the most potent compound, 1,3,6-trimethylpyrimido[5,4-*e*][1,2,4] triazine-5,7(1*H*,6*H*)-dione (**35G8**), was selected for further analysis and optimization.

We next used the thermal shift assay[15] to validate whether **35G8** stabilizes its presumed target, PDI. Intriguingly, **35G8** destabilized PDI, indicated by the decrease in melting temperature of the protein (Figure 2A). The dose-dependence of the negative thermal shifts at all concentrations tested (ΔT_m: −3.64 °C at 100 μM; −2.94 °C at 10 μM; −1.43 °C at 1 μM) (Fig-

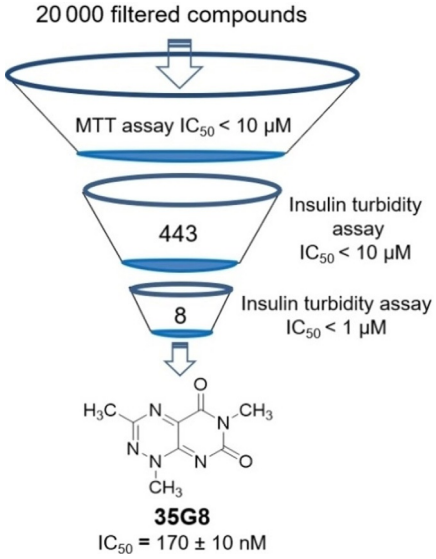

Figure 1. Discovery of **35G8**. Work flow summarizing the screening process that identified **35G8** as a potent PDI inhibitor; 20000 compounds were screened in an MTT assay with HCT116 cells and 443 compounds were cytotoxic in these cells. The 443 compounds were tested further in an insulin turbidity assay; **35G8** had the most potent IC_{50} value and was taken for further biochemical analysis and optimization.

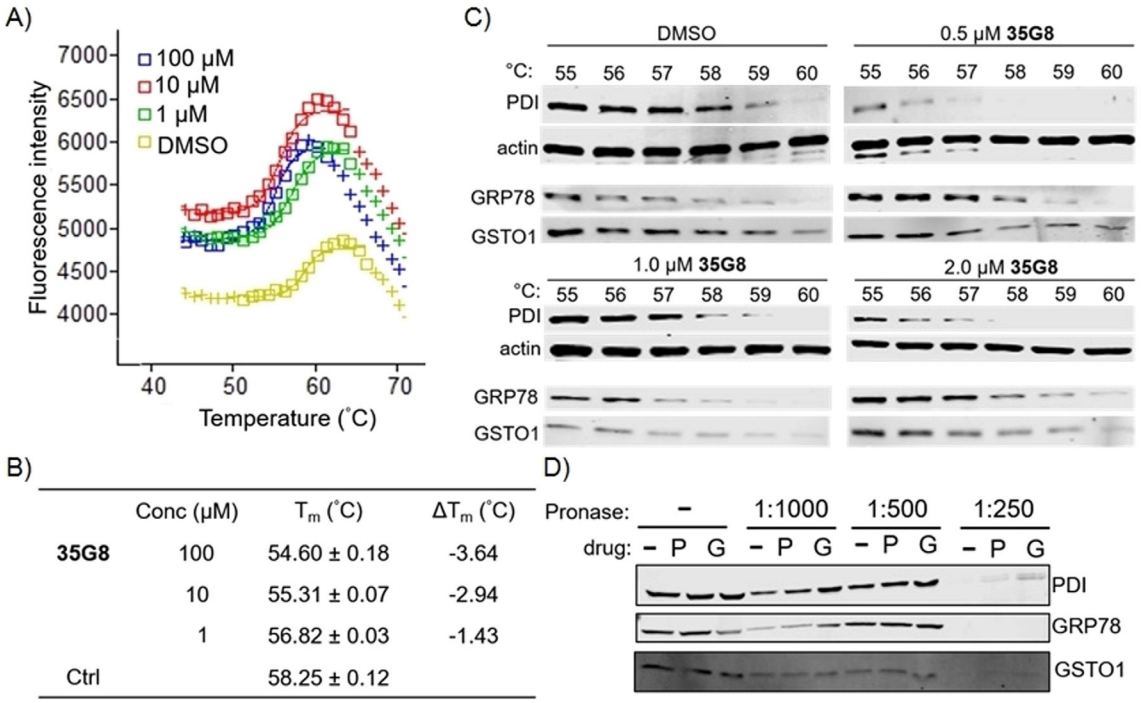

Figure 2. 35G8 destabilizes PDI. A) Thermal shifts observed for recombinant PDI (0.3 mg mL^{-1}) with various concentrations of **35G8**; DMSO was used as a control. B) Apparent melting temperatures (T_m) and change in melting temperature derived from ThermoFluor assay. C) Protein expression of PDI, GRP78, GSTO1, and actin (loading control) in the absence or presence of **35G8** at varying temperatures in the cellular thermal shift assay. D) Western blot analysis of DARTS assay with PDI, GRP78, and GSTO1 subjected to 100 μM **PACMA31** (P), 100 μM **35G8** (G), or DMSO (−). Samples were subjected to varying concentrations of pronase. Data are means from three independent experiments.

ure 2B) provides further evidence that **35G8** associates with and destabilizes PDI. The melting temperature of a protein shifts positively or negatively in the presence of a ligand, and this change in melting temperature parallels the stability of the protein.[16] These results suggest **35G8** interacts with PDI at a unique site relative to known stabilizing ligands, such as estradiol.[17] To further validate **35G8** binding to PDI, we performed the cellular thermal shift assay (CETSA) and drug affinity responsive target stability (DARTS) assay. **35G8** also destabilized PDI via CETSA (Figure 2C). **35G8** had little effect on a related molecular chaperone, GRP78, but did seem to stabilize the cysteine-containing glutathione-transferase Omega 1 (GSTO1). In the DARTS assay, U87MG cell lysates were subjected to pronase degradation in the presence or absence of **PACMA31** or **35G8** (Figure 2D). Both compounds protected PDI from proteolysis, but had no effect on the degradation of GRP78 or GSTO1. These results established **35G8** as a potent, selective inhibitor of PDI.

We further validated **35G8** as a bona fide PDI inhibitor by examining several of its close derivatives. Of the 16 analogues reported in the National Cancer Institute (NCI) database (Table S1), we pursued a refined group of eight compounds from the Developmental Therapeutics Program and tested their purity using UPLC–MS. Three of the eight compounds (NSC 67078, 99733 and 280172; hereafter referred to as **NC72**, **NC75**, and **NC79**, respectively) were over 95% pure and were tested in the insulin turbidity assay (Table 1).

We also synthesized several analogues of **35G8** to validate the above findings. The lead compound, **35G8**, contains methyl substituents at the three N1, C3, and N6 positions (Figure 1). We incorporated various substituents at the C3 position while maintaining the methyl groups at N1 and N6 due to the efficient introduction of the N1 and N6 methyl groups early in the synthesis (Scheme 1). Nucleophilic attack of methylhydrazine on 6-chloro-3-methyl uracil (**1**) led to hydrazinylpyrimidine-2,4(1*H*,3*H*)-dione (**2a**).[18] Further condensation with aldehydes furnished the corresponding hydrazones (**3a–f**). Each hydrazone was cyclized by treatment with sodium nitrite in acetic acid/water to afford a mixture of pyrimidotriazinediones (**4a–f**) and the corresponding *N*-oxide derivative (**5d**).

All **35G8** analogues had strong PDI inhibitory activity with sub-micromolar IC_{50} values, except **NC75** (>120 μM) and **NC79** (6.55±1.19 μM) in the insulin turbidity assay (Table 1). The pyrimidotriazinedione compound (**35G8**, IC_{50}: 0.17±0.01 μM) was more potent than the corresponding *N*-oxide compound (**NC79**). A similar trend was observed between **4d** (IC_{50}: 0.36±0.05 μM) and **5d** (IC_{50}: 0.42±0.07 μM). Among the pyrimidotriazinediones, the compounds containing a methyl group (**4a**) or no substituent (**NC72**) at R^1 had enhanced activity over those with an aromatic moiety (**4b–f**), likely due to steric effects (Figure S1A). Interestingly, the PDI inhibitory activity was abolished upon removal of the methyl substituent at R^2 (**NC75**: IC_{50} >120 μM) compared to **NC72** (IC_{50}: 0.105 μM), indicating that the methyl group at R^2 may be necessary to retain PDI inhibitory activity (Figure S1B). Furthermore, the removal of PDI inhibitory activity abolished the cytotoxicity of the compound.

Table 1. PDI inhibitory activity of **35G8** analogues.

Compd	A Basic Module	B R^1	R^2	IC_{50} [μM][h]
35G8 (**4a**)[a]	A	CH_3	CH_3	0.17±0.01
4b[b]	A		CH_3	0.39±0.03
4c[c]	A		CH_3	0.33±0.04
4d[d]	A	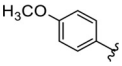	CH_3	0.36±0.05
4e[e]	A		CH_3	0.32±0.01
4f[f]	A	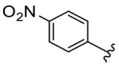	CH_3	0.24±0.04
5d[g]	B	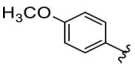	CH_3	0.42±0.07
NC72 (**NSC67078**)	A	H	CH_3	0.105±0.004
NC75 (**NSC99733**)	A	H	H	>120
NC79 (**NSC280172**)	B	CH_3	CH_3	6.55±1.19
PACMA31	–	–	–	5.81±1.23

[a] 1,3,6-Trimethylpyrimido[5,4-*e*][1,2,4]triazine-5,7(1*H*,6*H*)-dione. [b] 1,6-Dimethyl-3-phenylpyrimido[5,4-*e*][1,2,4]triazine-5,7(1*H*,6*H*)-dione. [c] 3-Benzyl-1,6-dimethylpyrimido[5,4-*e*][1,2,4]triazine-5,7(1*H*,6*H*)-dione. [d] 3-(4-Methoxyphenyl)-1,6-dimethylpyrimido[5,4-*e*][1,2,4]triazine-5,7(1*H*,6*H*)-dione. [e] 3-(3-Methoxyphenyl)-1,6-dimethylpyrimido[5,4-*e*][1,2,4]triazine-5,7(1*H*,6*H*)-dione. [f] 1,6-Dimethyl-3-(4-nitrophenyl)pyrimido[5,4-*e*][1,2,4]triazine-5,7(1*H*,6*H*)-dione. [g] 3-(4-Methoxyphenyl)-1,6-dimethyl-5,7-dioxo-1,5,6,7-tetrahydropyrimido[5,4-*e*][1,2,4]triazine 4-oxide. [h] Values obtained in insulin turbidity assays; data are the mean±SD from three independent experiments.

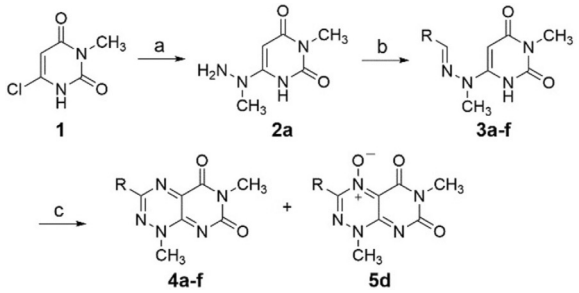

Scheme 1. Synthesis of 3-substituted **35G8** analogues: a) methylhydrazine, EtOH, reflux; b) aldehyde (R-CHO), anhydrous EtOH, room temperature; c) $NaNO_2$, $AcOH/H_2O$, room temperature.

35G8 analogues inhibit glioblastoma cell proliferation

All synthesized compounds demonstrated potent cytotoxicity in four glioblastoma cell lines, U87MG, U118MG, A172 and NU04, with IC_{50} values under 10 μM, except **4c** (Table 2). The

Table 2. In vitro cytotoxicity of **35G8** analogues in a panel of human glioblastoma cell lines.

Compd	IC_{50} [μM][a]			
	U87MG	U118MG	NU04	A172
35G8	1.1 ± 0.2	3.9 ± 0.1	0.8 ± 0.2	2.0 ± 0.6
4b	3.0 ± 0.3	4.6 ± 0.5	3.7 ± 1.2	1.8 ± 0.4
4c	12.7 ± 3.7	24.0 ± 7.4	> 30	8.2 ± 2.5
4d	1.2 ± 0.2	3.9 ± 0.6	0.86 ± 0.04	1.5 ± 0.4
4e	1.1 ± 0.2	2.4 ± 0.6	0.76 ± 0.22	1.5 ± 0.1
4f	1.8 ± 0.7	6.2 ± 1.6	4.9 ± 1.2	1.1 ± 0.2
5d	1.9 ± 0.7	4.3 ± 0.1	1.5 ± 0.7	1.7 ± 0.1
NC72	0.5 ± 0.1	–	–	–
NC75	> 100	–	–	–
NC79	> 100	–	–	–
PACMA31	0.13 ± 0.07	0.28 ± 0.04	0.4 ± 0.1	0.12 ± 0.10

[a] Cytotoxicity measured by MTT assay; data are the mean ± SD from at least three independent experiments.

IC_{50} value of **35G8** in U87MG cells is 1.1 ± 0.2 μM. **NC72** demonstrated the most potent cytotoxicity (IC_{50} = 0.5 ± 0.1 μM), complementing its potency in the PDI assay (Table 1). **NC75** and **NC79** had little effect on cell growth. Interestingly, this suggests that the methyl substituent is important not only for PDI activity (as seen in the dramatic IC_{50} value increase from **NC72** to **NC75**), but also for cytotoxicity.

Pretreatment with Z-VAD-FMK, an irreversible caspase inhibitor,[19] and necrostatin-1, a necroptosis inhibitor,[20] did not protect the cells from **35G8**-induced cell death (Figure S2A). These results indicate that neither necrosis nor apoptosis are the main pathways responsible and another pathway may be implicated in cell death.

35G8 may bind in the catalytic site of PDI

The pyrimidotriazinedione class may bind PDI catalytic sites preferentially and interact with the cysteine residues (Figure 3A–C). Interestingly, the compounds are predicted to bind the C-terminal C397 site over the sequence-identical N-terminal C53 site, likely due to the composition of a binding pocket around C397. Docking pose conformation of **35G8** in the C397 catalytic site and the corresponding PoseView26 representation illustrate hydrogen bonding and pi-pi interactions with important residues of the active site: K424, E391 and Y393 (Figure 3D). The synthesized analogues, an additional 409 analogues of **35G8**, and the **NC** compounds also bind in the N-terminal active site pocket, forming similar interactions (Figure S1B). The docking poses of the synthesized analogues (**4b–5d**) indicate that the larger substitution at R^1 is subject to steric hindrance that decreases potency (Figure S1A). **NC75** has the lowest docking score for binding to the catalytic site

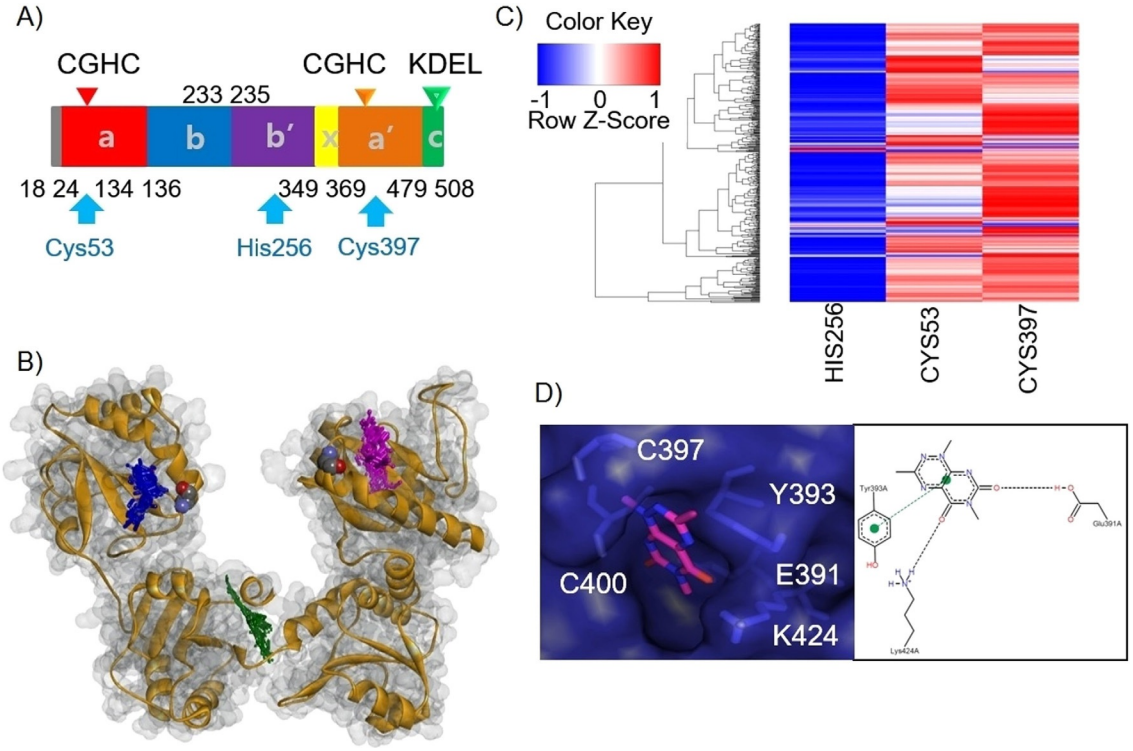

Figure 3. Docking of **35G8** analogues on PDI reveals their interaction with catalytic cysteine 397. A) Location of the three binding pockets on the domain architecture of PDI. B) Heat map plot for docking of 409 analogues of **35G8** in three binding pockets of PDI. C) Structural overview of ten **35G8** analogues docked in PDI binding sites. The catalytic cysteines are colored by atom in a space-filling representation. The rest of the protein is depicted in grey and orange. The docked structures are shown in purple, green and blue for the C53, H256, and C397 site, respectively. D) Docking pose of **35G8** in the C397 catalytic site of the PDI along with a PoseView representation showing its interactions with the binding site residues.

(Figure S1 B), in agreement with its inactivity in vitro. This suggests that the presence of a methyl group at the R^2 position is important for the hydrophobic interaction in the binding site.

35G8 induces the Nrf2 antioxidant pathway and ER stress response

To better elucidate the cellular response to the pyrimidotriazinediones, we performed nascent RNA sequencing using the Bru-seq[22] method and analyzed changes in gene transcription rates in response to **35G8** in U87MG cells. Four hours after **35G8** treatment, 498 genes were upregulated at least two-fold and 238 genes were downregulated at least two-fold. Many of the top upregulated genes are implicated in the Nrf2 antioxidant response, ER stress response, and autophagy. We identified the top 20 upregulated and downregulated gene sets (Tables S2 and S3) and analyzed the genes that were upregulated or downregulated at least two-fold with IPA (Ingenuity Pathway Analysis) (Figure 4 A and Table S4) and GSEA (Gene Set Enrichment Analysis) (Figure 4 B, Tables S5 and S6). GSEA snapshots of enriched gene sets are reported in Figures S3 and S4. GSEA revealed enrichment of the Nrf2-mediated oxidative stress response upon **35G8** treatment (Figure 4 B). Treatment also correlates with KOBAYASHI_EGFR_SIGNALING_24HR_DN gene set, suggesting **35G8** may inhibit EGFR signaling. DAVID (the Database for Annotation, Visualization and Integrated Discovery) analysis identified functional terms related to ER and redox-active disulfide, providing further evidence for PDI inhibition by **35G8** (Figure 4 C,D).

The upregulation of Nrf2 response genes, including HMOX1 (19-fold increase), SLC7A11 (63-fold increase), AKR1C1 (59-fold increase), and LOC344887 (23-fold increase), is likely a protective response to the insults caused by **35G8** (Figure 4 E). We also confirmed parallel increases in HMOX1 and SLC7A11 protein expression (Figure 4 F). The Nrf2 antioxidant pathway mitigates oxidative stress by inducing antioxidant response elements.[23] PDI is vital in the UPR, and inhibiting this key protein disrupts proteostasis, ultimately leading to ER stress and cell death when the cell cannot cope with the accumulation of misfolded proteins. ER stress target genes downstream the PERK-ATF4 ER stress response pathway, CHAC1 (46-fold increase), DDIT3 (4-fold increase), and HSPA5 (8-fold increase) increased as a result of **35G8** treatment (Figure 4 E). Protein expression of GRP78 (HSPA5) and DDIT3 increased upon 24-hour treatment of 2 μM **35G8** (Figure 4 G); however, CHAC1 protein was undetectable, likely because the CHAC1 protein is rapidly degraded by the proteasome (data not shown).[24] mRNA expression of other downstream targets of the PERK-ATF4 ER stress response pathway, including TRIB3 and ASNS,[25] also increased in response to **35G8** (Figure 4 E). These results suggest that brain cancer cells rely on PDI to maintain redox homeostasis, and when PDI is inhibited, cells undergo irremediable ER stress that leads to cell death.

We also identified several autophagic signaling genes that respond to ER stress triggered by **35G8**, including TRIB3, IRS2, and TMEM74 (Figure 4 E). TRIB3 (23-fold increase), as a downstream target of ATF4, mediates autophagy by inhibiting the mTORC1 pathway.[26] IRS2 (12-fold increase) activation induces protective autophagy to clear unwanted protein aggregates[27] and may also help remove damaged cells. TMEM74 (28-fold increase), a transmembrane protein localized to the lysosome and autophagosome, regulates autophagy.[28] The increased transcription of these autophagy-related genes prompted us to measure protein expression of several autophagy markers (Figure 4 H). Cleaved LC3B expression increased significantly after 24-hour treatment with 2 μM **35G8**, however expression levels of other autophagy markers, including ATG3, ATG5, ATG7, and beclin 1, did not change (data not shown), suggesting that autophagy may play a more protective role in this case. These results indicate that **35G8** induces the ER stress and Nrf2 response in brain cancer cells to contribute to cell death. GSEA analysis also showed that **35G8** treatment repressed many genes involved in DNA repair pathways such as mismatch repair, homologous recombination, base excision repair and nucleotide excision repair (Figure S5). Even though not all pathways showed significance individually in the GSEA analysis, the fact that all of them were suppressed suggests that the expression of these DNA repair genes is regulated by a common transcription factor that requires PDI-mediated folding for proper activity. These findings open up the interesting possibility that **35G8** could act synergistically with DNA-damaging agents and have therapeutic implications.

Bru-seq analysis identifies novel glioblastoma markers

AKR1C1, IL-6, CHAC1 and TNFSF9 are among the top 20 upregulated genes with significantly decreased expression in brain cancer relative to normal brain tissues (Figure 5 A–C). Conversely, genes that were downregulated upon **35G8** treatment, including TXNIP (−7.40-fold change), EGR1 (−5.65-fold change) and ITGA3 (−3.89-fold change) are often overexpressed in brain cancer (Figure 5 D–F). Additional genes affected include HMOX1, IRS2, SLC7A11, and mir181A2HG (Figure S6). These data suggest **35G8** inhibits transcription of these mRNA, or inhibits an upstream regulator of ITGA3 and EGR1. The results also indicate a gene such as IL6 may be used as a biomarker of **35G8** inhibition in future studies and EGR1 may be a novel glioblastoma marker.

35G8 induces ROS formation

Because the cells responded to **35G8** by upregulating the Nrf2-mediated oxidative stress response, we investigated the production of reactive oxygen species (ROS) by **35G8** and its analogues to determine whether the cytotoxicity of these compounds is dependent on ROS induction. We observed significant ROS induction by all **35G8** analogues tested at 5 μM as early as four hours after treatment, except for **4c** (Figure 6). ROS accumulation with these compounds was time-dependent. At 24 hours, 5 μM **35G8** treatment achieved maximal ROS induction, comparable to 100 μM hydrogen peroxide treatment (Figure 6 C). No change in the fluorescent signal in the samples containing **35G8** without H_2DCFDA dye was observed, eliminating the possibility of endogenous fluorescence

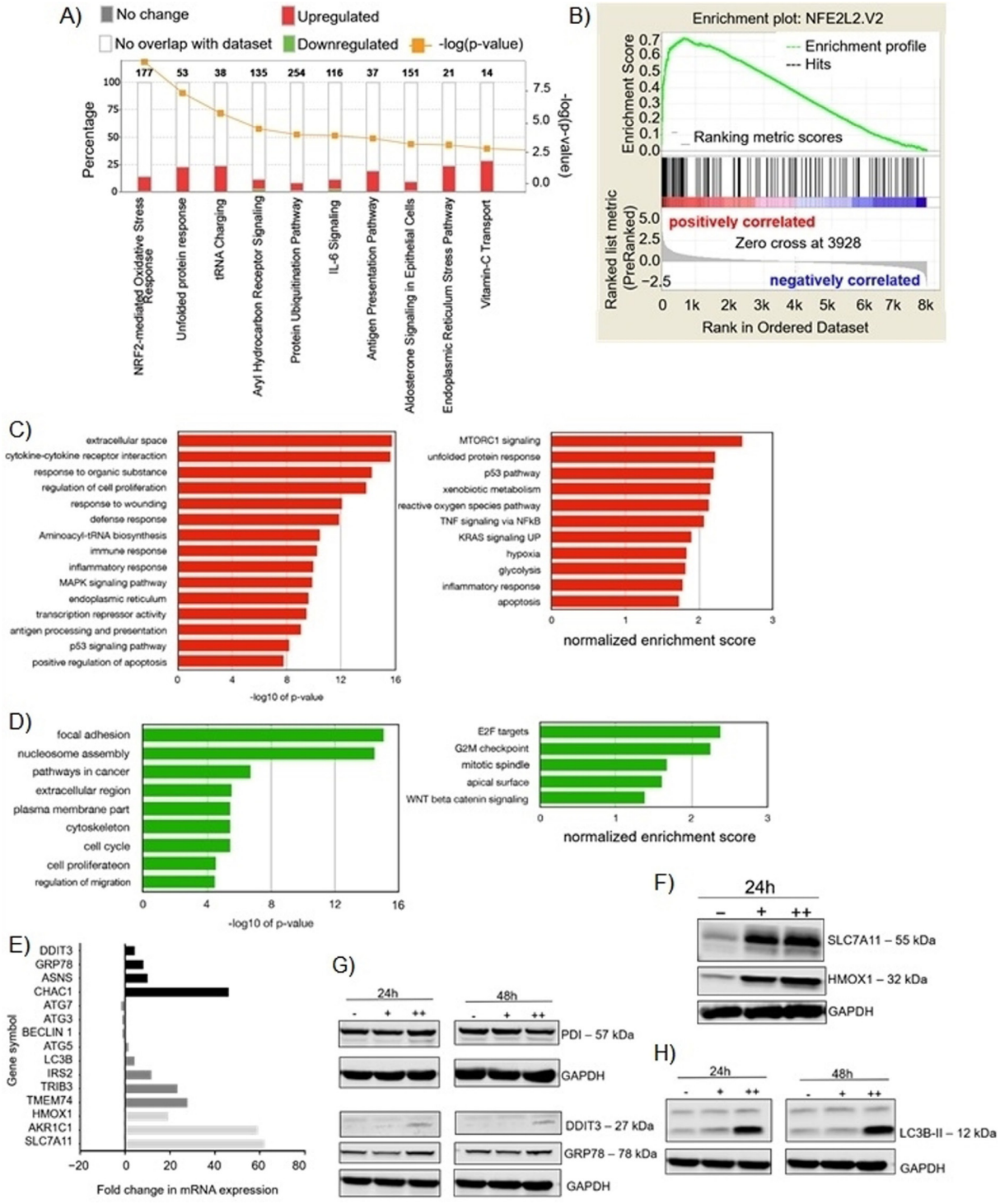

Figure 4. Effects of **35G8** treatment on cellular pathways. A) Pathways from the Bru-seq analysis of **35G8**-treated cells. B) GSEA for "NFE2L2.V2," the top gene set matched with upregulated genes from Bru-seq results. Functional terms represented by genes upregulated (C) and downregulated (D) at least twofold by **35G8** treatment. Pathway analysis was performed using DAVID (left) and GSEA (right). E) Histograms of differentially expressed proteins between **35G8**-treated and DMSO-treated U87MG cells. Fold change bars are in black for UPR genes, dark grey for autophagy-related genes, and light grey for Nrf2-related genes. F) Western blot showing Nrf2-regulated proteins SLC7A11 and HMOX1 expression upon 24-hour treatment of U87MG cells with 1 or 2 μM **35G8**. GAPDH used as a loading control. G) Western blot of ER stress-induced proteins DDIT3 and GRP78 expression upon 24 hour treatment of U87MG cells with 1 and 2 μM **35G8**. GAPDH used as a loading control. H) Western blot of autophagy-related proteins LC3B, beclin 1, ATG3, ATG5, and ATG7 expression upon 24 hour treatment of U87MG cells with 1 (+) and 2 (++) μM **35G8**; vehicle-treated control: (−). GAPDH was used as a loading control; experiments were repeated in triplicate.

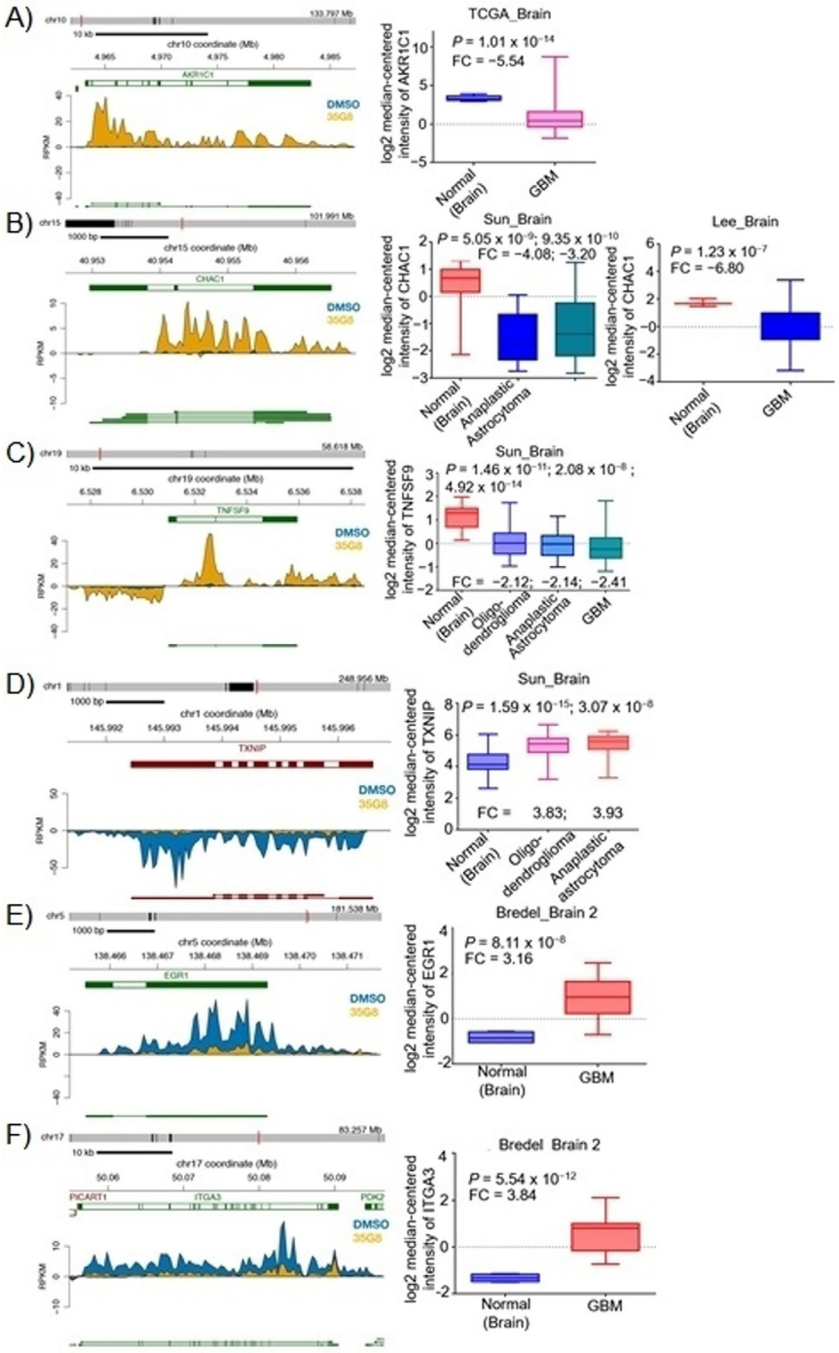

Figure 5. Effect of **35G8** treatment on RNA synthesis in U87MG cells. **35G8** induces transcription of A) AKR1C1, B) CHAC1 and C) TNFSF9 while corresponding box plots show downregulation of these genes in brain cancer. **35G8** inhibits the transcription of D) TXNIP, E) EGR1 and F) ITGA3 while corresponding box plots show upregulation of these genes in brain cancer. FC: fold change; GBM: glioblastoma.

affecting the assay. *N*-acetylcysteine (NAC) did not affect the cytotoxicity of **35G8** significantly (Table S7). This suggests **35G8**-induced cell death is not solely dependent on ROS induction.

35G8 induces ferroptosis

Both transcription and protein expression of HMOX1 and SLC7A11 are highly upregulated by **35G8** (Figure 4E,F). These proteins have been implicated in the non-apoptotic cell death mechanism, ferroptosis. HMOX1 is necessary for ferroptosis and is a major source of iron in the body.[29] Inhibition of cysteine-glutamate exchange through system x^{c-}, of which SLC7A11 is a component, induces iron-dependent cell death.[30] To determine whether **35G8** induces ferroptosis in U87MG cells, we treated the cells in the presence or absence of deferoxamine (DFO), an iron chelator (Figure S2B).[31] In the presence of DFO, **35G8** is almost three times less potent (IC_{50} =

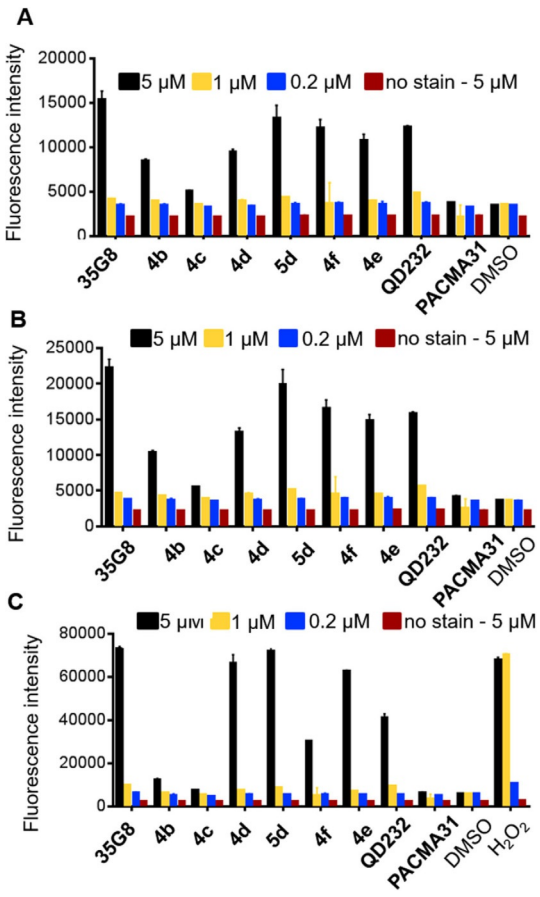

Figure 6. ROS induction activity of synthesized **35G8** analogues at A) 4, B) 6, and C) 24 h. In panel C), hydrogen peroxide concentration is 500, 100, and 20 μM, from left to right. Data are means from three independent experiments; error bars show standard deviation.

5.8 ± 1.0 μM) than when used alone (IC_{50} = 2.2 ± 0.7 μM). These data suggest that PDI may play an important role in preventing ferroptosis in brain cancer.

35G8 is expected to cross the blood–brain barrier

The likelihood of blood–brain barrier (BBB) permeation, Alog*P*, water solubility, polar surface area, and number of rotatable bonds of **35G8** and its synthesized analogues were determined with a qualitative model in the ADMET predictor (Version 7.0) (Table S8; Figure S8). The Alog*P* of the compounds is between −1.1 and 1.1 and the likelihood of BBB permeation is high. The polar surface area of **35G8** is less than 90 Å^2, the cutoff for predicted CNS penetration.[32] The average molecular weight of marketed CNS compounds is 310, and the **35G8** analogues range in molecular weight from 207–315. Similarly, TMZ has a molecular weight of 194 Da, Clog*P* of −0.82, and a polar surface area of 108 Å^2. These data demonstrate that **35G8** will be able to cross the blood–brain barrier.

Discussion

The screen of 20 000 diverse compounds in a growth inhibition assay produced **35G8** as the most potent inhibitor of proliferation of the colon cancer cell line HCT116. **35G8** destabilizes PDI and blocks its reductase activity. As a consequence, **35G8** likely causes cell death via continuous activation of ER stress and disruption of homeostatic balance, among other factors. **35G8** was validated in orthogonal assays to rule out that activity was not a consequence of its redox-cycling status. **35G8** generates H_2O_2 in the presence of DTT at the concentrations used in the PDI assay (Figure S9 A), however, H_2O_2 does not interfere with insulin reduction catalyzed by PDI (Figure S9 B). The reactive nature of the pyrimidotriazinedione class underlines the importance of testing activity in a wide variety of assays, including non-fluorescent methods, in order to eliminate false positive results. Therefore, we performed several assays with various output methods to test our novel compounds.

The Bru-seq results revealed that **35G8** promoted the activation of the Nrf2 pathway. Of the top 20 upregulated genes following a 4-hour **35G8** treatment, four are implicated in the Nrf2 pathway (SLC7A11, HMOX1, AKR1C1, and LOC344887). Nrf2 is a transcription factor that normally is kept at low levels due to degradation mediated via Keap1.[33] Following exposure to ROS, Keap1 is inactivated and Nrf2 induces transcription of genes, counteracting the oxidative insult.[34] SLC7A11 is part of a cysteine-glutamate transporter (system x^{c-}) that is regulated by Nrf2 as well as ATF4.[35] HMOX1, another Nrf2-regulated gene, increased over 19-fold upon **35G8** treatment. We also found that transcription of the AKR1C1 gene, which is induced by ROS but expressed at low levels in gliomas, increased significantly following **35G8** treatment. Furthermore, the lncRNA LOC344887 has been shown to be activated by Nrf2.[36] Nrf2-regulated genes may be responsible for treatment resistance in glioblastoma, providing further evidence that inhibiting PDI could be a sound strategy to treat glioblastoma.[37]

Several ER stress markers were induced in response to **35G8** treatment, including CHAC1, DDIT3, ASNS, and ATF3. Due to the strong upregulation of CHAC1, a pro-apoptotic marker regulated by ATF4, we hypothesize that the PERK-ATF4-DDIT3 branch of the UPR is likely activated upon PDI inhibition by **35G8** treatment. The ER stress response and autophagy are closely linked, and ER stress may induce autophagy in **35G8**-treated cells.

Autophagy is the process of protein and organelle degradation by lysosomes, used as a survival mechanism to provide energy for the cell.[38] The ER stress response protein ATF4 promotes autophagy[39] by upregulating genes like TRIB3.[40] While autophagy can be protective as a survival mechanism, increased autophagic signaling causes cell death. It is still unclear whether TMEM74 is regulated by ATF4, but upregulation of TMEM74 mRNA may lead to autophagic PI3K signaling. The increase of ARG2 expression upon **35G8** treatment may be a result of the activation of the UPR and lower cellular levels of arginine, leading to autophagy.[41] IRS2, a key insulin signaling protein regulated by the UPR and silenced by JNK, is expressed

to remove damaged cells.[42] **35G8** treatment initiates a protective response by upregulating the UPR and inducing autophagy to combat ER stress. Ultimately, the unbalanced homeostatic mechanisms overwhelm the cellular machinery, and this leads to cell death.

ROS induction is likely responsible for the increased expression levels of TXNRD1 (9-fold increase) and TXN (2-fold increase). TXNIP inhibits TXN activity and TXNIP expression is significantly inhibited by **35G8** treatment (7.4-fold decrease). ER stress activates the ERK1/2 MAP kinase signaling pathway, repressing TXNIP expression leading to thioredoxin nuclear translocation.[43] Interestingly, TXNIP is overexpressed in brain cancer patients. TXNIP also can bind PDI and increase its activity.[43] Lower TXNIP levels allow TRX to bind ASK1 and prevent apoptosis.[44] Therefore, decreased expression of TXNIP may contribute to the absence of apoptosis signaling observed upon **35G8** treatment.

Another class of genes that were repressed by **35G8** are involved in DNA repair (Figure S5). While this repression was not dramatic, GSEA analysis showed that several genes involved in mismatch repair, homologous recombination, base excision repair and nucleotide excision repair showed decreased transcription following **35G8** treatment. It is possible that these genes share a common transcription factor that requires PDI-assisted protein folding for optimal function. Importantly, these findings suggest that **35G8** may be used in combination with DNA damaging agents or PARP1 inhibitors to augment their therapeutic effectiveness.

The key Nrf2-regulated genes SLC7A11 and HMOX1 are essential markers for iron-dependent, erastin-induced ferroptosis.[29,30] SLC7A11 is a negative regulator of ferroptosis and upregulation of SLC7A11 occurs as a response to system x^{c-} inhibition.[13] Efforts to treat glioma patients by inhibiting system x^{c-} have failed;[45] however, combining SLC7A11 inhibition with a PDI inhibitor may be a promising new strategy. Importantly, **35G8**-induced cell death can be rescued by deferoxamine, suggesting that ferroptosis is occurring.

System x^{c-} imports cystine for glutathione synthesis[13] to maintain intracellular redox balance and the expression of this system is often elevated in several cancers, including gliomas.[46] System x^{c-} inhibitors, in particular sulfasalazine, as single agents for the treatment of gliomas have been unsuccessful,[47] but have been shown to sensitize glioma cells to radiation therapy.[48] Similarly, the ferroptosis inducer erastin sensitizes glioblastoma cells to temozolomide by inhibiting system x^{c-}.[49] These studies provide evidence that system x^{c-} is an important target for combating resistance in brain cancer. Interestingly, Bru-seq analysis of **35G8**-treated cells revealed a pattern of gene expression similar to that of erastin-treated cells (Figure S9), including induction of the ER stress response, unfolded protein response, and expression of the erastin-exposure pharmacodynamic marker, CHAC1.[50] This indicates that as a consequence of PDI inhibition, **35G8** is causing blockade of system x^{c-}. However, a link between PDI and SLC7A11 expression has not yet been established and further investigation is warranted.

Conclusions

We identified **35G8** as a markedly potent PDI inhibitor that may have therapeutic potential as a single agent and in combination with SLC7A11 inhibitors or DNA-damaging agents. **35G8** and its analogues demonstrate activity in human brain cancer cells likely through upregulation of ER stress and UPR that leads to autophagy-mediated ferroptosis. Taken together, our data suggest **35G8** is a useful investigational PDI inhibitor, expected to easily cross the blood brain barrier, that can be optimized to develop novel therapeutic agents to treat malignant glioma.

Experimental Section

Chemistry

All commercial chemicals and solvents were reagent grade and were used without further purification unless otherwise specified. Analytical thin layer chromatography was performed on Merck precoated plates (silica gel 60 F_{254}) to follow the course of reactions. Proton nuclear magnetic resonance (^{1}H NMR) spectroscopy was performed on Bruker Ascend 400 MHz spectrometer or Varian 500 MHz spectrometer. Chemical shifts (δ) are reported in parts per million (ppm) units relative to residual undeuterated solvent. The following abbreviations are used to describe peak splitting patterns when appropriate: s (singlet), d (doublet), t (triplet), q (quartet), m (multiplet), bs (broad singlet), dd (doublet of doublets), dt (doublet of triplets). Coupling constants (*J*) are expressed in Hertz (Hz). Low-resolution mass spectra were recorded on a Thermo-Scientific LCQ Fleet mass spectrometer or a Micromass LCT time-of-flight instrument using the electro spray ionization (ESI) mode. HPLC was used to determine the purity of biologically tested compounds using the Shimadzu HPLC Test Kit C18 column (3 μm, 4.6 × 50 mm) under the following gradient elution conditions: mobile phase A of acetonitrile/water (10–95 %) or mobile phase B of methanol/water (10–95 %). The purity of three NCI compounds (**NC72**, **NC75**, and **NC79**) was determined by ultra-performance liquid chromatography (UPLC). UPLC was carried out using Acquity UPLC BEH (C18-1.7 μm, 2.1 mm × 50 mm) with a gradient elution of acetonitrile/water (10–100 %). The purity was established by integration of the areas of major peaks detected at 254 nm, and all tested compounds including three **NC** compounds have ≥ 95 % purity.

3-Methyl-6-(1-methylhydrazinyl)pyrimidine-2,4(1*H*,3*H*)-dione (2 a): A solution of 6-chloro-3-methyluracil (2.01 g, 12.5 mmol), methylhydrazine (2.87 g, 62.3 mmol) and absolute ethanol (30 mL) was heated at reflux for 3 hours. The reaction mixture was cooled to room temperature, and the precipitate was collected, washed with ethanol, and dried to give **2 a** as a white solid (819 mg, 39 %). ^{1}H NMR (400 MHz, [D$_6$]DMSO): δ = 7.64 (bs, 1 H), 4.75 (s, 1 H), 3.33 (bs, 2 H), 3.03 (s, 3 H), 2.43 ppm (s, 3 H); MS (ESI) *m/z* = 171 $[M+H]^+$.

3-Methyl-6-(1-methylhydrazinyl)pyrimidine-2,4(1*H*,3*H*)-dione (3 a): To a suspension of **2 a** (3.18 g, 18.7 mmol) in absolute ethanol (30 mL) was added acetaldehyde (1.65 g, 37.4 mmol) at room temperature with stirring. The reaction mixture was stirred for 2 hours, and the precipitate was filtered off by suction, washed with ethanol, and dried to give **3 a** as an off-white solid (823 mg, 22 %). ^{1}H NMR (400 MHz, $CDCl_3$): δ = 9.21 (bs, 1 H), 7.08 (q, *J* = 5.2 Hz, 1 H), 5.00 (d, *J* = 2.4 Hz, 1 H), 3.31 (s, 3 H), 3.16 (s, 3 H), 2.09 ppm (s, 3 H); MS (ESI) *m/z* = 197 $[M+H]^+$.

6-(2-Benzylidene-1-methylhydrazinyl)-3-methylpyrimidine-2,4(1*H*,3*H*)-dione (3b): The same procedure for the synthesis of compound **3a** was followed using compound **2a** (500 mg, 2.94 mmol) and benzaldehyde (636 mg, 5.88 mmol) as reactants to yield **3b** as a beige solid (590 mg, 78%). ^{1}H NMR (500 MHz, [D$_6$]DMSO): δ = 10.64 (s, 1H), 7.97 (s, 1H), 7.96 (d, J = 6.5 Hz, 2H), 7.44–7.38 (m, 3H), 5.24 (s, 1H), 3.34 (s, 3H), 3.10 ppm (s, 3H); MS (ESI) m/z = 259 $[M+H]^+$.

3-Methyl-6-(1-methyl-2-(2-phenylethylidene)hydrazinyl)pyrimidine-2,4(1*H*,3*H*)-dione (3c): The same procedure for the synthesis of compound **3a** was followed using compound **2a** (500 mg, 2.94 mmol) and phenyl acetaldehyde (744 mg, 5.88 mmol) as reactants. The crude compound was further purified by recrystallization from ethanol to yield **3c** as a white brilliant solid (427 mg, 53%). ^{1}H NMR (500 MHz, $CDCl_3$): δ = 9.18 (s, 1H), 7.36 (t, J = 7.3 Hz, 2H), 7.29 (t, J = 7.4 Hz, 1H), 7.21 (d, J = 7.3 Hz, 2H), 7.09 (t, J = 5.7 Hz, 1H), 5.02 (d, J = 2.5 Hz, 1H), 3.70 (d, J = 5.7 Hz, 2H), 3.31 (s, 3H), 3.14 ppm (s, 3H); MS (ESI) m/z = 273 $[M+H]^+$.

6-(2-(4-Methoxybenzylidene)-1-methylhydrazinyl)-3-methylpyrimidine-2,4(1*H*,3*H*)-dione (3d): The same procedure for the synthesis of compound **3a** was followed using compound **2a** (300 mg, 1.76 mmol) and 4-methoxybenzaldehyde (490 mg, 3.52 mmol) as reactants. The crude compound was further purified by recrystallization from ethanol to yield **3d** as a light-beige solid (241 mg, 47%). ^{1}H NMR (500 MHz, $CDCl_3$): δ = 9.18 (s, 1H), 7.66 (s, 1H), 7.63–7.60 (m, 2H), 6.98–6.94 (m, 2H), 5.10 (d, J = 2.5 Hz, 1H), 3.87 (s, 3H), 3.32 ppm (s, 6H); MS (ESI) m/z = 289 $[M+H]^+$.

6-(2-(3-Methoxybenzylidene)-1-methylhydrazinyl)-3-methylpyrimidine-2,4(1*H*,3*H*)-dione (3e): The same procedure for the synthesis of compound **3a** was followed using compound **2a** (200 mg, 1.17 mmol) and 3-methoxybenzaldehyde (320 mg, 2.35 mmol) as reactants. The crude compound was further purified by recrystallization from ethanol to yield **3e** as an off-white solid (90 mg, 27%). ^{1}H NMR (500 MHz, $CDCl_3$): δ = 9.16 (s, 1H), 7.66 (s, 1H), 7.35 (t, J = 7.9 Hz, 1H), 7.26–7.23 (m, 1H), 7.18–7.17 (m, 1H), 6.97 (dt, J = 8.2, 1.7 Hz, 1H), 5.13 (d, J = 2.5 Hz, 1H), 3.86 (s, 3H), 3.34 (s, 3H), 3.32 ppm (s, 3H); MS (ESI) m/z = 289 $[M+H]^+$.

3-Methyl-6-(1-methyl-2-(4-nitrobenzylidene)hydrazinyl)pyrimidine-2,4(1*H*,3*H*)-dione (3f): The same procedure for the synthesis of compound **3a** was followed using compound **2a** (140 mg, 0.82 mmol) and 4-nitrobenzaldehyde (254 mg, 1.65 mmol) as reactants. The crude compound was immediately used in the next step.

1,3,6-Trimethylpyrimido[5,4-*e*][1,2,4]triazine-5,7(1*H*,6*H*)-dione (4a): A stirring solution of the hydrazone **3a** (823 mg, 4.19 mmol) in glacial acetic acid (10 mL)/water (0.6 mL) cooled to 0 °C was treated with sodium nitrite (895 mg, 12.6 mmol). The reaction mixture was allowed to warm to room temperature while stirring. Stirring continued until TLC indicated consumption of the starting material, thereby furnishing a mixture of the pyrimidotriazinedione (**4a**) and the corresponding *N*-oxide derivative. The reaction mixture was diluted with water and extracted with dichloromethane. The combined organic layers were dried over sodium sulfate, and the solvent was evaporated in vacuo. The resulting residue was chromatographed on silica to afford the product **4a** as a brilliant yellow solid (272 mg, 31%). ^{1}H NMR (500 MHz, $CDCl_3$): δ = 4.11 (s, 3H), 3.49 (s, 3H), 2.75 ppm (s, 3H); MS (ESI) m/z = 208 $[M+H]^+$; HPLC (mobile phase A): purity 99.9%.

1,6-Dimethyl-3-phenylpyrimido[5,4-*e*][1,2,4]triazine-5,7(1*H*,6*H*)-dione (4b): The same procedure for the synthesis of compound **4a** was followed using the hydrazone **3b** (300 mg, 1.16 mmol) and sodium nitrite (247 mg, 3.48 mmol) as reactants to afford the product **4b** as an orange solid (112 mg, 36%). ^{1}H NMR (500 MHz, $CDCl_3$): δ = 8.32 (dd, J = 8.1, 1.6 Hz, 2H), 7.56–7.52 (m, 3H), 4.24 (s, 3H), 3.53 ppm (s, 3H); MS (ESI) m/z = 270 $[M+H]^+$; HPLC (mobile phase A): purity 95.0%.

3-Benzyl-1,6-dimethylpyrimido[5,4-*e*][1,2,4]triazine-5,7(1H,6*H*)-dione (4c): The same procedure for the synthesis of compound **4a** was followed using the hydrazone **3c** (300 mg, 1.10 mmol) and sodium nitrite (235 mg, 3.30 mmol) as reactants. The crude product was purified by column chromatography and further recrystallized from ethanol to afford the product **4c** as an oil (100 mg, 32%). ^{1}H NMR (500 MHz, $CDCl_3$): δ = 7.38–7.25 (m, 5H), 4.29 (s, 2H), 4.11 (s, 3H), 3.47 ppm (s, 3H); MS (ESI) m/z = 284 $[M+H]^+$; HPLC (mobile phase A): purity 98.6%.

3-(4-Methoxyphenyl)-1,6-dimethylpyrimido[5,4-e][1,2,4]triazine-5,7(1*H*,6*H*)-dione (4d): The same procedure for the synthesis of compound **4a** was followed using the hydrazone **3d** (220 mg, 0.763 mmol) and sodium nitrite (163 mg, 2.29 mmol) as reactants. The crude product was purified by column chromatography and further recrystallized from ethanol to afford the product **4d** as a red solid (81 mg, 35%). ^{1}H NMR (500 MHz, $CDCl_3$): δ = 8.25 (d, J = 8.9 Hz, 2H), 7.00 (d, J = 8.9 Hz, 2H), 4.21 (s, 3H), 3.89 (s, 3H), 3.52 ppm (s, 3H); MS (ESI) m/z = 300 $[M+H]^+$; HPLC (mobile phase A): purity 96.1%.

3-(3-Methoxyphenyl)-1,6-dimethylpyrimido[5,4-*e*][1,2,4]triazine-5,7(1*H*,6*H*)-dione (4e): The same procedure for the synthesis of compound **4a** was followed using the hydrazone **3e** (77 mg, 0.267 mmol) and sodium nitrite (70 mg, 0.801 mmol) as reactants to afford the product **4e** as a yellow solid (15 mg, 19%). ^{1}H NMR (500 MHz, $CDCl_3$): δ = 7.91 (d, J = 7.7 Hz, 1H), 7.79 (s, 1H), 7.42 (t, J = 7.9 Hz, 1H), 7.08 (d, J = 7.6 Hz, 1H), 4.23 (s, 3H), 3.90 (s, 3H), 3.52 ppm (s, 3H); MS (ESI) m/z = 300 $[M+H]^+$; HPLC (mobile phase B): purity 97.2%.

1,6-Dimethyl-3-(4-nitrophenyl)pyrimido[5,4-*e*][1,2,4]triazine-5,7(1*H*,6*H*)-dione (4f): The same procedure for the synthesis of compound **4a** was followed using the crude hydrazone **3f** (69 mg, 0.227 mmol) and sodium nitrite (60 mg, 0.683 mmol) as reactants to afford the product **4f** as an orange solid (18 mg, 25%). ^{1}H NMR (500 MHz, $CDCl_3$): δ = 8.51 (d, J = 8.9 Hz, 2H), 8.37 (d, J = 8.9 Hz, 2H), 4.27 (s, 3H), 3.53 ppm (s, 3H); MS (ESI) m/z = 313 $(M\text{-}H)^-$; HPLC (mobile phase A): purity 96.8%.

3-(4-Methoxyphenyl)-1,6-dimethyl-5,7-dioxo-1,5,6,7-tetrahydropyrimido[5,4-*e*][1,2,4]triazine 4-oxide (5d): Following the same procedure for the synthesis of the pyrimidotriazinedione (**4d**), the corresponding *N*-oxide derivative was isolated by column chromatography to afford the product **5d** as an orange solid (90 mg, 37%). ^{1}H NMR (500 MHz, $CDCl_3$): δ = 7.86 (d, J = 9.0 Hz, 2H), 6.99 (d, J = 8.9 Hz, 2H), 4.07 (s, 3H), 3.89 (s, 3H), 3.42 ppm (s, 3H); MS (ESI) m/z = 316 $[M+H]^+$; HPLC (mobile phase A): purity 98.1%.

Biological assays

Reagents: 3-(4,5-dimethylthiazol-2-yl)-2, 5-diphenyltetrazolium bromide (MTT) was purchased from Amresco (Solon, OH). *N*-acetylcysteine (NAC) was purchased from Sigma–Aldrich (St. Louis, MO, USA). Methyl (3*S*)-5-fluoro-3-[[(2*S*)-2-[[(2*S*)-3-methyl-2-(phenylmethoxycarbonylamino)butanoyl]amino]propanoyl]amino]-4-oxopentanoate (Z-VAD-FMK) was purchased from Tocris Bioscience (Bristol, UK). 5-(1*H*-Indol-3-ylmethyl)-3-methyl-2-sulfanylideneimidazolidin-4-one (Necrostatin-1) was purchased from Cayman Chemical Compa-

ny (Ann Arbor, MI, USA). Phenol red, H_2O_2, and horseradish peroxidase (HRP) were purchased from Sigma–Aldrich (St. Louis, MO, USA). Hank's Balanced Salt Solution (HBSS) was purchased from Hyclone, Logan, UT (USA), and sodium hydroxide was purchased from EMD, Gibbstown, NJ (USA).

Cell culture: The human glioblastoma cells, U87MG, U118MG, NU04 and A172 (ATCC, Manassas, VA, USA), were obtained in 2013, and were maintained in RPMI-1640 (Thermo Fisher Scientific, Waltham, MA, USA) with 10% fetal bovine serum (Thermo Fisher Scientific). Cells were grown as monolayer cultures at 37 °C in a humidified atmosphere of 5% CO_2 and tested for *Mycoplasma* contamination with the Mycoplasma Detection Kit, PlasmoTest (InvivoGen, San Diego, CA, USA).

Growth inhibition assay: Cell growth inhibition was assessed by MTT assay as previously described.[51] Cells were seeded in duplicate in 96-well plates at 7000–10 000 cells per well. After overnight incubation at 37 °C and 5% CO_2, cells were treated with indicated compounds for 72 hours. For the combination therapies, NAC was added to the well at the same time as **35G8** (24 hours after plates were seeded), and Z-VAD-FMK and Necrostatin-1 were added to the well 1 hour prior to **35G8** addition. The plates were incubated with drug or vehicle control for 72 hours at 37 °C and 5% CO_2. MTT solution (20 μL 3 mg mL^{-1}) was added to the wells, and the cells were incubated for 4 hours at 37 °C. Supernatant was removed and DMSO (100 μL) was added to each well. The plates were shaken for 15 minutes at room temperature and absorbance of the formazan crystals was measured at 570 nm. Cell growth inhibition was assessed by the cell viability rate as $[1-(A_t-A_b)/(A_c-A_b)]\times 100$ (for which A_t, A_c, and A_b are the absorbance values from cells treated with compound, cells not treated with compound, and blank, respectively). Cell viability was determined with the MTT assay. U87MG cells were seeded at 5000 cells per well in 96-well plates. Deferoxamine (Sigma–Aldrich) was added to cells in a five-point, three-fold dilution series from 400 μM. **35G8** was added immediately after in a five-point, three-fold dilution series from 100 μM. Cells were incubated with compounds for 12 hours at 37 °C, and MTT assay was performed as stated above.

PDI protein purification: The expression vector of recombinant human PDI protein with N-terminal His tag was a gift from Dr. Lloyd W. Ruddock (University of Oulu, Oulu, Finland). PDI expression and purification were performed as previously described[5] with slight modifications. In brief, protein production was carried out in *Escherichia coli* strain BL21 (DE3) pLysS grown in LB medium with 200 μg mL^{-1} ampicillin (EMD Biosciences, La Jolla, CA, USA) at 37 °C and incubated at an A600 of 0.5 for 4 hours with 1 mM isopropyl β-D-1-thiogalactopyranoside (GoldBio, St. Louis, MO, USA). Cells were harvested by centrifugation (4000×*g* for 15 min) and were resuspended in one-tenth volume Buffer A (20 mM sodium phosphate, pH 7.3). Cells were lysed by sonication and the cell debris was removed by centrifugation (16 000×*g* for 30 min). The supernatant was applied to a bed of Ni-nitrilotriacetic acid in a histidine-binding column (Qiagen, Hilden, Germany), equilibrated with 10 mL of Buffer A and incubated at 4 °C, overnight. After incubation, the column was washed in Buffer A and then in Buffer B (20 mM sodium phosphate, 0.5 M sodium chloride and 50 mM imidazole, pH 7.3). His-tagged proteins were eluted using Buffer C (20 mM sodium phosphate and 50 mM EDTA, pH 7.3) and eluent was dialyzed in 100 mM sodium phosphate buffer (pH 7.0) with 2 mM EDTA.

Measurement of PDI activity: PDI activity was assessed by measuring the PDI-catalyzed reduction of insulin as described previously.[14] In brief, recombinant PDI protein (0.4 μM) was incubated with indicated compounds at 37 °C for 1 hour in sodium phosphate buffer (100 mM sodium phosphate, 2 mM EDTA, 8 μM DTT, pH 7.0). A mixture of sodium phosphate buffer, DTT (500 μM), and bovine insulin (130 μM; Gemini BioProducts, West Sacramento, CA) was added to the incubated PDI protein. The reduction reaction was catalyzed by PDI at room temperature, and the resulting aggregation of reduced insulin B chains was measured at 620 nm. Percent PDI activity was calculated with the formula: PDI activity (%) = $[(OD_{T80}[PDI+DTT+compound]-OD_{T0}[PDI+DTT+compound])-(OD_{T80}[DTT]-OD_{T0}[DTT])]/[(OD_{T80}[PDI+DTT]-OD_{T0}[PDI+DTT])-(OD_{T80}[DTT]-OD_{T0}[DTT])]\times 100$ (for which OD_{T0} and OD_{T80} are the absorbance values at 0 and 80 min after the reduction reaction, respectively).

Thermal shift assay: Thermal shift of purified PDI (0.3 mg mL^{-1} in 100 mM $NaPO_4$, pH 7.0) in the presence or absence of **35G8** was determined as described.[15] Briefly, 5 μL protein dye (1,8-ANS, 0.3 mM; Sigma–Aldrich, St. Louis, MO, USA) solutions were dispensed in each well of a 384-well microplate (Thermo Scientific, AB1384K) and equal volumes of the test compound solutions were dispensed to each well. Then, 3 μL of silicone oil (Sigma–Aldrich, St. Louis, MO, USA) was added to each well to prevent evaporation. DMSO (2% in buffer) was used as control. Fluorescence emission was detected by measuring light intensity using a CCD camera. The plate was heated at a temperature range from 25 to 90 °C at 1 °C min^{-1} in the ThermoFluor instrument (Johnson & Johnson, New Brunswick, NJ, USA). Compounds were replicated three times in a 384-well plate.

Cellular thermal shift assay: The cellular thermal shift assay was performed following previously established procedure.[52] U87MG cells were seeded at 2×10^6 cells per 100 mm dish and allowed to attach overnight. Cells were treated with 0.5, 1.0, or 2.0 μM **35G8**, or DMSO as the negative control, for 2 hours at 37 °C, 5% CO_2. After treatment, cells were trypsinized, washed with DPBS twice, and suspended in 600 μL DPBS. The cells were split into 100 μL aliquots, heated at indicated temperatures for 3 minutes in the Veriti Thermal Cycler (Applied Biosystems), and incubated for 3 minutes at room temperature. The cells were flash-frozen twice and spun at 14×*g* for 20 minutes at 4 °C. Supernatants were collected and loaded onto a 10% polyacrylamide gel at a volume of 16 μL, with 4 μL 4× SDS loading dye. Subsequently, western blotting was run following the procedure reported herein.

Drug affinity responsive target stability: The DARTS assay was performed following previously established procedure.[53] U87MG cells were grown to ~80–85% confluence, washed with ice-cold DPBS, and lysed with lysis buffer (150 mM NaCl, 1.0% NP-40, 0.5% sodium deoxycholate, 50 mM Tris, pH 8.0). Cells were collected and lysis was allowed to occur for 10 minutes on ice. Cells were spun at 18 000×*g* for 20 minutes at 4 °C to collect the supernatant. Protein concentration was determined via BCA assay. 100 μM **PACMA31** or **35G8** or 1 μL DMSO were incubated with aliquots of cell lysate at 5 mg mL^{-1} for 30 minutes with shaking at room temperature. Pronase (Sigma–Aldrich, St. Louis, MO, USA) was added to 20 μL aliquots of cell lysates at 0, 1:1000 (0.005 μg μL^{-1}), 1:500 (0.01 μg μL^{-1}), or 1:250 (0.02 μg μL^{-1}) for 30 minutes at room temperature. Digestion was stopped by adding 1× protease inhibitor cocktail (Sigma–Aldrich, St. Louis, MO, USA) and incubating the reactions on ice for 10 minutes. SDS-PAGE loading buffer (6 μL of 5×) was added to the samples, and samples were heated for 10 minutes at 70 °C. Samples were spun down briefly and 20 μg of protein was loaded into acrylamide gels (10%) for western blot analysis.

Docking study: Docking studies were performed using GOLD, version 4.0 (Cambridge Crystallographic Data Centre).[54] The crystal structure of human PDI in its reduced state (PDB ID: 4EKZ)[55] was used for all calculations. 3D structures of the ligands were created and energy minimized using MMFF94 force-field implemented in OMEGA 2.5.1.4 (OpenEye Scientific Software, http://www.openeye.com), a systematic, knowledge-based conformer generator.[21] The docking site was defined for all residues within 10 Å around the center, defined as the sulfur atoms of the catalytic residues Cys53 and Cys397 and nitrogen NE2 of His256 for the hydrophobic site. Docking studies were performed using the standard default settings with 100 GA (genetic algorithm) runs on each molecule. Gold Score was used to quantify the interactions between molecules and PDI and the annealing parameters with cutoff values of 3.0 Å for hydrogen bonds and 4.0 Å for van der Waals interactions were used as default. When the top three solutions attained RMSD values within 1.5 Å, docking was terminated. During the docking process, a maximum of 10 conformers was considered for each compound.

Bru-seq analysis: Bru-seq experiments[12] and analysis were performed as previously reported. Briefly, U87MG cells were placed in dishes on Day 1. Cells were changed to fresh media on Day 5 and treated with DMSO or **35G8** at 1 μM for 4 hours. Bromouridine was added into the media to a final concentration of 2 mM to label newly synthesized nascent RNA in the last 30 minutes of treatment. Cells were then collected in TRIzol (Thermo Fisher Scientific, Waltham, MA) and total RNA was isolated. The bromouridine-containing RNA population was further isolated and sequenced. Sequencing reads were mapped to a reference genome.

Bioinformatic analysis: Bru-seq data of **35G8** treatment was filtered using the cut off value of gene size >300 bp and mean (RPKM) >0.5 and a total of 7770 genes were ranked based on the fold change values versus control (DMSO). DAVID functional annotation analysis[56] was performed on 460 upregulated and 220 downregulated genes with fold change ≥ 2 and ≤ -2. IPA of Bru-seq data was performed using the IPA web-based application (Ingenuity Systems, Inc.) on the list of 680 up- and downregulated genes (over two-fold change) (Tables S4 and S5). Top canonical pathways were ranked based on the P-value of significance and maximum number of genes in the pathway (Figure 4A). Gene Set Enrichment Analysis (GSEA) of Bru-seq data was done on a pre-ranked gene list of 7770 genes of **35G8** treatment based on the Kolmogorov-Smirnov statistic.[57] Table S3 and S4 show the top 20 gene sets for up- and downregulated genes of the Bru-seq dataset of **35G8** treatment, respectively. The snapshots of the enrichment profiles of these 20 gene sets are provided in Figure S4 and S5.

ROS detection assay: U87MG cells were detached with 0.05% trypsin-EDTA (Thermo Fisher Scientific, Waltham, MA), neutralized, centrifuged and resuspended in cell culture media. Suspension was treated with 20 μM cell-permeable H_2DCFDA (Thermo Fisher Scientific, Waltham, MA, USA) for 30 minutes at 37 °C. Cells were centrifuged again and washed with cell culture media to remove excess probe. After washing, cells were placed in a black-wall 384-well plate at 20000 cells per well, incubated for 30 minutes and treated with compounds at designated conditions. Fluorescent signals were read at 493 nm/523 nm for ROS detection at designated time points (4, 6, and 24 hours).

Western blot: Primary antibodies for GRP78, HMOX1, CHAC1, CHOP, LC3B, GSTO1, and SLC7A11 and secondary antibodies were purchased from Cell Signaling (Danvers, MA, USA). Primary antibody for P4HB was purchased from Protein Tech (Rosemont, IL, USA). U87MG cells were treated with DMSO or 2 μM **35G8** for 1, 3, 6, 12, or 24 hours. Cells were harvested with a lysis buffer (25 mM tris(hydroxymethyl)aminomethane, 150 mM NaCl, 17 mM Triton X-100, 3.5 mM SDS, pH 7.4), lysed via sonication, and spun in a centrifuge at 13,500×*g* at 4 °C for 10 minutes. Supernatant was collected and protein concentration determined with the BCA assay (Thermo Fisher Scientific, Waltham, MA, USA). Samples were prepared with 50 μg protein and loaded onto 10% (or 12% for LC3B and DDIT3) acrylamide (Bio-Rad, Hercules, CA, USA) gels. Protein from gels was electro-transferred to methanol-activated immobilon-FL PVDF membranes (EMD Millipore, La Jolla, CA, USA). Membranes were blocked for 1 hour with Odyssey Blocking Buffer (LI-COR Biosciences, Lincoln, NE, USA). Membranes were probed for proteins using primary antibodies (P4HB, 1:1000; GRP78, 1:1000; GSTO1, 1:1000; HMOX1, 1:1000; CHAC1, 1:1000; CHOP, 1:500; LC3B, 1:2000; SLC7A11, 1:2000) overnight at 4 °C. Membranes were incubated with secondary antibodies (anti-rabbit, 1:7500, or anti-mouse, 1:7500) and fluorescence was imaged by Odyssey Imaging Systems (LI-COR Biosciences).

Redox cycling assay: The redox cycling assay was adapted from a previously published experiment.[58] In duplicate in a 384-well plate, 20 μL of HBSS buffer, 100 U of catalase, 100 μM H_2O_2, 100 μM H_2O_2 + 100 U catalase, 0.5% DMSO, 500 μM DTT, 10 μM **35G8**, 10 μM **35G8** + 500 μM DTT, or 10 μM **35G8** + 500 μM DTT + 100 U of catalase was added to a reaction mixture with HBSS to a final volume of 60 μL. The reaction was incubated at room temperature for 30 minutes, and phenol red-HRP detection reagent was added to a final concentration of 100 μg mL^{-1} phenol red and 60 μg mL^{-1} HRP in each well. The reaction was incubated for an hour at room temperature. Sodium hydroxide (10 μL, 1 N) was added to wells and absorbance was measured at 610 nm.

Statistical analysis: IC_{50} values were calculated using GraphPad Prism 7 software (GraphPad Software, Inc.). Error bars indicate mean ± standard deviation.

Acknowledgements

The authors thank Michelle Paulsen for running the Bru-seq experiments. The expression vector of recombinant human PDI was a generous gift from Dr. Lloyd W. Ruddock (University of Oulu, Oulu, Finland). This work was supported in part by a grant from the US National Institutes of Health (NIH; grant no. CA193690).

Conflict of interest

The authors declare no conflict of interest.

Keywords: cancer · drug discovery · oxidoreductases · protein disulfide isomerase · unfolded protein response

[1] Q. T. Ostrom, H. Gittleman, P. Liao, C. Rouse, Y. W. Chen, J. Dowling, Y. L. Wolinsky, C. Kruchko, J. Barnholtz-Sloan, *Neuro-Oncology* **2014**, *16*, 1–63.

[2] R. Stupp, W. P. Mason, M. J. van den Bent, M. Weller, B. Fisher, M. J. Taphoorn, K. Belanger, A. A. Brandes, C. Marosi, U. Bogdahn, J. Curschmann, R. C. Janzer, S. K. Ludwin, T. Gorlia, A. Allgeier, D. Lacombe, J. G. Cairncross, E. Eisenhauer, R. O. Mirimanoff, European Organisation for Research and Treatment of Cancer Brain Tumor and Radiotherapy Groups; National Cancer Institute of Canada Clinical Trials Group, *N.*

Engl. J. Med. **2005**, *352*, 987 – 996; National Cancer Institute of Canada Clinical Trials Group, *N. Engl. J. Med.* **2005**, *352*, 987 – 996.
[3] S. Xu, S. Sankar, N. Neamati, *Drug Discovery Today* **2014**, *19*, 222 – 240.
[4] a) L. Ellgaard, L. W. Ruddock, *EMBO Rep.* **2005**, *6*, 28 – 32; b) A. Shergalis, N. Neamati in *Encyclopedia of Signaling Molecules* (Ed.: S. Choi), Springer, New York, **2016**, pp. 1 – 12.
[5] S. Xu, A. N. Butkevich, R. Yamada, Y. Zhou, B. Debnath, R. Duncan, E. Zandi, N. A. Petasis, N. Neamati, *Proc. Natl. Acad. Sci. USA* **2012**, *109*, 16348 – 16353.
[6] D. Goplen, J. Wang, P. Enger, B. B. Tysnes, A. J. Terzis, O. D. Laerum, R. Bjerkvig, *Cancer Res.* **2006**, *66*, 9895 – 9902.
[7] P. E. Lovat, M. Corazzari, J. L. Armstrong, S. Martin, V. Pagliarini, D. Hill, A. M. Brown, M. Piacentini, M. A. Birch-Machin, C. P. Redfern, *Cancer Res.* **2008**, *68*, 5363 – 5369.
[8] J. Eirich, S. Braig, L. Schyschka, P. Servatius, J. Hoffmann, S. Hecht, S. Fulda, S. Zahler, I. Antes, U. Kazmaier, S. A. Sieber, A. M. Vollmar, *Angew. Chem. Int. Ed.* **2014**, *53*, 12960 – 12965; *Angew. Chem.* **2014**, *126*, 13174 – 13179.
[9] C. Khodier, L. VerPlank, P. P. Nag, J. Pu, J. Wurst, T. Pilyugina, C. Dockendorff, C. N. Galinski, A. A. Scalise, F. Passam, L. van Hessem, J. Dilks, D. R. Kennedy, R. Flaumenhaft, M. A. J. Palmer, S. Dandapani, B. Munoz, S. L. Schrieber in *Probe Reports from the NIH Molecular Libraries Program*, Bethesda, MD (USA), **2010**.
[10] A. Kaplan, M. M. Gaschler, D. E. Dunn, R. Colligan, L. M. Brown, A. G. Palmer, D. C. Lo, B. R. Stockwell, *Proc. Natl. Acad. Sci. USA* **2015**, *112*, E2245 – E2252.
[11] S. Vatolin, J. G. Phillips, B. K. Jha, S. Govindgari, J. Hu, D. Grabowski, Y. Parker, D. J. Lindner, F. Zhong, C. W. Distelhorst, M. R. Smith, C. Cotta, Y. Xu, S. Chilakala, R. R. Kuang, S. Tall, F. J. Reu, *Cancer Res.* **2016**, *76*, 3340 – 3350.
[12] M. T. Paulsen, A. Veloso, J. Prasad, K. Bedi, E. A. Ljungman, B. Magnuson, T. E. Wilson, M. Ljungman, *Methods* **2014**, *67*, 45 – 54.
[13] S. J. Dixon, K. M. Lemberg, M. R. Lamprecht, R. Skouta, E. M. Zaitsev, C. E. Gleason, D. N. Patel, A. J. Bauer, A. M. Cantley, W. S. Yang, B. Morrison III, B. R. Stockwell, *Cell* **2012**, *149*, 1060 – 1072.
[14] M. M. Khan, S. Simizu, N. S. Lai, M. Kawatani, T. Shimizu, H. Osada, *ACS Chem. Biol.* **2011**, *6*, 245 – 251.
[15] M. W. Pantoliano, E. C. Petrella, J. D. Kwasnoski, V. S. Lobanov, J. Myslik, E. Graf, T. Carver, E. Asel, B. A. Springer, P. Lane, F. R. Salemme, *J. Biomol. Screening* **2001**, *6*, 429 – 440.
[16] P. Cimmperman, L. Baranauskienė, S. Jachimovičiūtė, J. Jachno, J. Torresan, V. Michailovienė, J. Matulienė, J. Sereikaitė, V. Bumelis, D. Matulis, *Biophys. J.* **2008**, *95*, 3222 – 3231.
[17] T. P. Primm, H. F. Gilbert, *J. Biol. Chem.* **2001**, *276*, 281 – 286.
[18] a) G. D. Daves, C. C. Cheng, R. K. Robins, *J. Am. Chem. Soc.* **1961**, *83*, 3904 – 3905; b) T. Nagamatsu, H. Yamasaki, T. Hirota, M. Yamato, Y. Kido, M. Shibata, F. Yoneda, *Chem. Pharm. Bull.* **1993**, *41*, 362 – 368.
[19] A. Degterev, Z. H. Huang, M. Boyce, Y. Q. Li, P. Jagtap, N. Mizushima, G. D. Cuny, T. J. Mitchison, M. A. Moskowitz, J. Y. Yuan, *Nat. Chem. Biol.* **2005**, *1*, 112 – 119.
[20] A. Degterev, J. Hitomi, M. Germscheid, I. L. Ch'en, O. Korkina, X. Teng, D. Abbott, G. D. Cuny, C. Yuan, G. Wagner, S. M. Hedrick, S. A. Gerber, A. Lugovskoy, J. Yuan, *Nat. Chem. Biol.* **2008**, *4*, 313 – 321.
[21] P. C. D. Hawkins, A. G. Skillman, G. L. Warren, B. A. Ellingson, M. T. Stahl, *J. Chem. Inf. Model.* **2010**, *50*, 572 – 584.
[22] M. T. Paulsen, A. Veloso, J. Prasad, K. Bedi, E. A. Ljungman, Y. C. Tsan, C. W. Chang, B. Tarrier, J. G. Washburn, R. Lyons, D. R. Robinson, C. Kumar-Sinha, T. E. Wilson, M. Ljungman, *Proc. Natl. Acad. Sci. USA* **2013**, *110*, 2240 – 2245.
[23] K. Itoh, T. Chiba, S. Takahashi, T. Ishii, K. Igarashi, Y. Katoh, T. Oyake, N. Hayashi, K. Satoh, I. Hatayama, M. Yamamoto, Y. Nabeshima, *Biochem. Biophys. Res. Commun.* **1997**, *236*, 313 – 322.
[24] K. Oh-hashi, Y. Nomura, K. Shimada, H. Koga, Y. Hirata, K. Kiuchi, *Mol. Cell. Biochem.* **2013**, *380*, 97 – 106.
[25] a) Y. Y. Shang, M. Zhong, L. P. Zhang, Z. X. Guo, Z. H. Wang, Y. Zhang, J. T. Deng, W. Zhang, *Clin. Exp. Pharmacol. Physiol.* **2010**, *37*, 51 – 55; b) F. Siu, P. J. Bain, R. LeBlanc-Chaffin, H. Chen, M. S. Kilberg, *J. Biol. Chem.* **2002**, *277*, 24120 – 24127.
[26] M. Salazar, A. Carracedo, I. J. Salanueva, S. Hernandez-Tiedra, M. Lorente, A. Egia, P. Vazquez, C. Blazquez, S. Torres, S. Garcia, J. Nowak, G. M. Fimia, M. Piacentini, F. Cecconi, P. P. Pandolfi, L. Gonzalez-Feria, J. L. Iovanna, M. Guzman, P. Boya, G. Velasco, *J. Clin. Invest.* **2009**, *119*, 1359 – 1372.
[27] A. Yamamoto, M. L. Cremona, J. E. Rothman, *J. Cell Biol.* **2006**, *172*, 719 – 731.
[28] C. F. Yu, L. Wang, B. F. Lv, Y. Lu, L. Zeng, Y. Y. Chen, D. L. Ma, T. P. Shi, *Biochem. Biophys. Res. Commun.* **2008**, *369*, 622 – 629.
[29] M.-Y. Kwon, E. Park, S.-J. Lee, S. W. Chung, *Oncotarget* **2015**, *6*, 24393 – 24403.
[30] S. J. Dixon, D. N. Patel, M. Welsch, R. Skouta, E. D. Lee, M. Hayano, A. G. Thomas, C. E. Gleason, N. P. Tatonetti, B. S. Slusher, B. R. Stockwell, *eLife* **2014**, *3*, e02523.
[31] J. M. C. Gutteridge, R. Richmond, B. Halliwell, *Biochem. J.* **1979**, *184*, 469 – 472.
[32] H. van de Waterbeemd, G. Camenisch, G. Folkers, J. R. Chretien, O. A. Raevsky, *J. Drug Targeting* **1998**, *6*, 151 – 165.
[33] K. Itoh, N. Wakabayashi, Y. Katoh, T. Ishii, K. Igarashi, J. D. Engel, M. Yamamoto, *Genes Dev.* **1999**, *13*, 76 – 86.
[34] G. T. Wondrak, *Antioxid. Redox Signaling* **2009**, *11*, 3013 – 3069.
[35] a) R. J. Bridges, N. R. Natale, S. A. Patel, *Br. J. Pharmacol.* **2012**, *165*, 20 – 34; b) M. Koritzinsky, B. G. Wouters, *Semin. Radiat. Oncol.* **2013**, *23*, 252 – 261.
[36] G. Johnson, L. Beaver, D. E. Williams, E. Ho, R. H. Dashwood in Thirteenth Annual AACR International Conference on Frontiers in Cancer Prevention Research, *Vol. 8*, *Can. Prev. Res.*, New Orleans, LA (USA), **2015**.
[37] a) J. H. Zhu, H. D. Wang, Y. W. Fan, Y. X. Lin, L. Zhang, X. J. Ji, M. L. Zhou, *Oncol. Rep.* **2014**, *32*, 443 – 450; b) J. H. Zhu, H. D. Wang, Q. Sun, X. J. Ji, L. Zhu, Z. X. Cong, Y. Zhou, H. D. Liu, M. L. Zhou, *BMC Cancer* **2013**, *13*, 380.
[38] B. Levine, *Nature* **2007**, *446*, 745 – 747.
[39] W. B'chir, A. C. Maurin, V. Carraro, J. Averous, C. Jousse, Y. Muranishi, L. Parry, G. Stepien, P. Fafournoux, A. Bruhat, *Nucleic Acids Res.* **2013**, *41*, 7683 – 7699.
[40] M. Salazar, M. Lorente, A. Orea-Soufi, D. Dávila, T. Erazo, J. Lizcano, A. Carracedo, E. Kiss-Toth, G. Velasco, *Biochem. Soc. Trans.* **2015**, *43*, 1122 – 1126.
[41] R. García-Navas, M. Munder, F. Mollinedo, *Autophagy* **2012**, *8*, 1557 – 1576.
[42] L. Xu, G. A. Spinas, M. Niessen, *Horm. Metab. Res.* **2010**, *42*, 643 – 651.
[43] F. T. Ogata, W. L. Batista, A. Sartori, T. F. Gesteira, H. Masutani, R. J. Arai, J. Yodoi, A. Stern, H. P. Monteiro, *PLoS One* **2013**, *8*, e84588.
[44] S. Lee, S. M. Kim, R. T. Lee, *Antioxid. Redox Signaling* **2013**, *18*, 1165 – 1207.
[45] P. A. Robe, D. H. Martin, M. T. Nguyen-Khac, M. Artesi, M. Deprez, A. Albert, S. Vanbelle, S. Califice, M. Bredel, V. Bours, *BMC Cancer* **2009**, *9*, 372.
[46] W. J. Chung, S. A. Lyons, G. M. Nelson, H. Hamza, C. L. Gladson, G. Y. Gillespie, H. Sontheimer, *J. Neurosci.* **2005**, *25*, 7101 – 7110.
[47] P. W. Gout, A. R. Buckley, C. R. Simms, N. Bruchovsky, *Leukemia* **2001**, *15*, 1633 – 1640.
[48] L. Sleire, B. S. Skeie, I. A. Netland, H. E. Forde, E. Dodoo, F. Selheim, L. Leiss, J. I. Heggdal, P. H. Pedersen, J. Wang, P. O. Enger, *Oncogene* **2015**, *34*, 5951 – 5959.
[49] L. Chen, X. Li, L. Liu, B. Yu, Y. Xue, Y. Liu, *Oncol. Rep.* **2015**, *33*, 1465 – 1474.
[50] S. J. Dixon, D. Patel, M. Welsch, R. Skouta, E. Lee, M. Hayano, A. G. Thomas, C. Gleason, N. Tatonetti, B. S. Slusher, B. R. Stockwell, *eLife* **2014**, *3*, e02523.
[51] J. Carmichael, W. G. DeGraff, A. F. Gazdar, J. D. Minna, J. B. Mitchell, *Cancer Res.* **1987**, *47*, 936 – 942.
[52] R. Jafari, H. Almqvist, H. Axelsson, M. Ignatushchenko, T. Lundback, P. Nordlund, D. M. Molina, *Nat. Protoc.* **2014**, *9*, 2100 – 2122.
[53] B. Lomenick, R. W. Olsen, J. Huang, *ACS Chem. Biol.* **2011**, *6*, 34 – 46.
[54] G. Jones, P. Willett, R. C. Glen, A. R. Leach, R. Taylor, *J. Mol. Biol.* **1997**, *267*, 727 – 748.
[55] C. Wang, W. Li, J. Ren, J. Fang, H. Ke, W. Gong, W. Feng, C. C. Wang, *Antioxid. Redox Signaling* **2013**, *19*, 36 – 45.
[56] a) G. Dennis, B. T. Sherman, D. A. Hosack, J. Yang, W. Gao, H. C. Lane, R. A. Lempicki, *Genome Biol.* **2003**, *4*, 3; b) D. W. Huang, B. T. Sherman, R. A. Lempicki, *Nat. Protoc.* **2009**, *4*, 44 – 57.

[57] A. Subramanian, P. Tamayo, V. K. Mootha, S. Mukherjee, B. L. Ebert, M. A. Gillette, A. Paulovich, S. L. Pomeroy, T. R. Golub, E. S. Lander, J. P. Mesirov, *Proc. Natl. Acad. Sci. USA* **2005**, *102*, 15545 – 15550.

[58] P. A. Johnston, K. M. Soares, S. N. Shinde, C. A. Foster, T. Y. Shun, H. K. Takyi, P. Wipf, J. S. Lazo, *Assay Drug Dev. Technol.* **2008**, *6*, 505 – 518.

Manuscript received: October 9, 2017
Revised manuscript received: December 10, 2017
Accepted manuscript online: December 12, 2017
Version of record online: January 4, 2018